PAPER • OPEN ACCESS

Numerical conjugate problem solution algorithm for fluid-deformable body system

Numerical conjugate problem solution algorithm for fluid-deformable body system

A P Zhukov, S V Belov[1], S V Ponomarev

National Research Tomsk State University, 36 Lenina Avenue, 634050, Tomsk, Russia

[1]E-mail: belovsv@niipmm.tsu.ru

Abstract. This paper describes the numerical conjugate problem solution algorithm for fluid-deformable body system. It is based on respective subtasks according to physical principals. To solve these subtasks, independent "black box" program modules are used. These modules are connected by conjugate conditions. Fluid phase domain boundary interface is discrete movable i.e. it is not movable on the integration time step, but its position is adjusted on the next time step.

1. Introduction

One type of conjugate problems could be considered as the interaction between fluid/gas flow and deformable solid body. In this problem formulation, there are at least two physical mediums. In this case, different sets of physical values, differential equations and boundary conditions are applied. Nevertheless, these mediums could not be regarded independently of each other. This interaction occurs on the boundary interface (BI) of adjacent regions which is mathematically formulated on the basis of conjugation conditions i.e. continuity of such values as forces, velocities, thermal flows etc. on the BI. As a result of the interaction of different physical factors, BI mediums could be displaced and deformed which, in its turn, should be included in the problem statement.

The growing interest in conjugate problems is determined by further improvement of solid-fuel rocket engines (SFRE) design structure.

One of the first publications describing numerical solution of conjugate problems was [1] (M. Kumar and K.K. Kuo). This paper discusses convective combustion within a deformed crack of SFRE solid-fuel charge. The authors subdivided the problem into three tasks:

- gas phase flow described on the basis of gas dynamics one-dimensional non-stationary equations;
- deformed solid phase state determined in two-dimensional stationary formulation;
- non-stationary thermal state of solid phase defined in one-dimensional formulation.

The gas and solid phase interaction on the BI was described by respective calculation algorithm.

Gas pressure and temperature were external loads for the solid phase, boundary changes of solid-fuel due to combustions and its deformations were regarded in the correction of crack section position.

Subdividing the conjugate problem according to physical processes, made it possible to resolve the functional compatibility problem of Euler and Lagrange methods. Moreover, it promoted the application of independent program solutions for above-mentioned tasks, including specific software packages which were connected by exchange data procedure. This approach was also described in [2-5].

The main issue in solving conjugate problem is the calculation fluid phase flow field taking into consideration boundaries motion of the specified region. The majority of numerical methods applied in calculating fluid phase flow field were based on the assumption that its boundaries are not movable. On the basis of these methods, quite a number of successfully software programs were developed. Simultaneously, when determining stress-strain of a solid phase, there is not a problem of its boundary motion consideration because of the fact that Lagrangian approach was used. However, it should be noted that the accepted Arbitrary Lagrangian-Eulerian method included the boundary motion of the fluid phase directly [3-5].

In a special case, conjugate problem could be considered as a problem of a non-deformed solid body motion in fluid or gas [6-7]. Thus, determining the stress-strain state of a solid body is not relevant.

The aim of this paper is to develop a numerical conjugate algorithm for fluid-deformable body system. It is based on the application of existing software programs. It is presupposed that the fluid phase on the time interval $[t;\ t+\Delta t]$ is determined under the condition that of its non-movable boundaries. Applied software programs to calculate fluid and solid phases are regarded as "black boxes", in which input data are geometry and structure of space grids, physico-mechanical phase characteristics, initial boundary conditions at point of time t, while output data include results describing phase states at point of time $t+\Delta t$.

If the boundary motion of solid phase is continuous during time step Δt, fluid boundary motion is discrete. This implies that within the time interval $[t;\ t+\Delta t]$ the fluid phase corresponds to point of time t, while within the next time interval it will correspond to point of time $t+\Delta t$. BI motion is regarded in the formulation of boundary condition as fluid or gas flow with corresponding velocities. New fluid phase position is determined by stress-strain state of solid phase calculation results, while the adjustment of fluid phase BI position is performed in specific programme module, and afterwards, written in initial data file as well as other programme data in order to make the calculations on the next time step.

2. Problem statement

Let's consider fluid-deformable solid body system in spatial domain Ω. This domain is subdivided into $\Omega_F \in \Omega$ (fluid phase subdomain) and $\Omega_S \in \Omega$ (solid phase subdomain), whereas $\Omega = \Omega_F \cup \Omega_S$. Both subdomains have common BI Γ, which is illustrated in figure1.
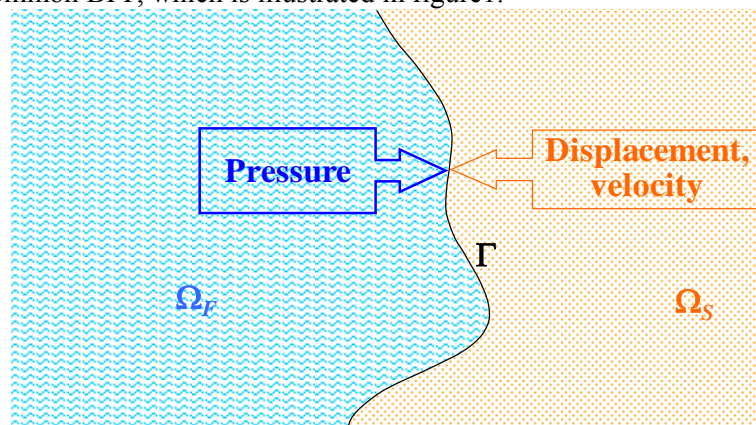

Figure 1. Fluid-deformable body system: Ω_F – fluid subdomain; Ω_S – deformable solid body subdomain; Γ – subdomain BI.

Both subdomains interact on Γ. Flow field of subdomain $\Omega_F(t)$ acts on the solid surface, which, in its turn, contacts with the fluid (on Γ). As a result, the solid body within $\Omega_S(t)$ is deformed, while Γ between the two mediums changes. Conversely, changed Γ acts on the fluid flow within $\Omega_F(t)$.

Thus, medium states of $\Omega_F(t)$ and $\Omega_S(t)$ are defined by the alignment of the parameter characteristics (pressures, stress, displacement velocity etc.) on Γ at every point of time.

In the case of moving subdomain $\Omega_F(t)$ within movable boundary $\partial\Omega_F(t)$, mass conservation law for Lagranginan representation is:

$$\frac{d}{dt}\int_{\Omega_F(t)}\rho_F(t)d\Omega + \int_{\partial\Omega_F(t)}\rho_F(t)\cdot(\upsilon - \upsilon_\Gamma)\cdot n\cdot dS = 0 \qquad (1)$$

where, υ – fluid velocity vector on $\partial\Omega_F(t)$; υ_Γ – boundary velocity vector on Γ; n – normal vector for boundary area element dS; ρ_F – fluid density.

For finite-difference representation, derivative of t from equation (1) is:

$$\frac{d}{dt}\int_{\Omega_F[t]}\rho_F[t]d\Omega \approx \frac{1}{\Delta t}\left(\int_{\Omega_F[t+\Delta t]}\rho_F[t+\Delta t]d\Omega - \int_{\Omega_F[t]}\rho_F[t]d\Omega\right) \qquad (2)$$

where, $[t]$ – corresponding point of time.

As Γ deforms, increment $\delta\Omega_F$ emerges within time interval from $[t; t+\Delta t]$ in subdomain $\Omega_F(t)$ as illustrated in figure 2:

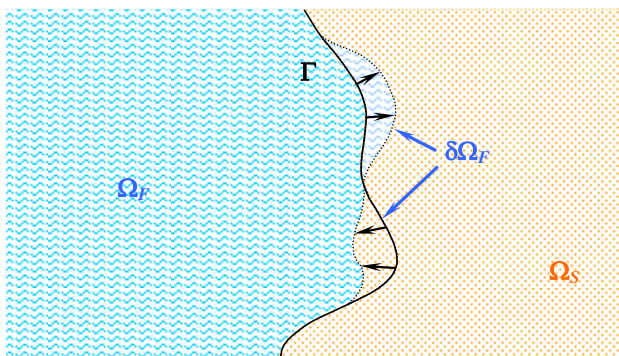$$\Omega_F[t+\Delta t] = \Omega_F[t] + \delta\Omega_F(t, \Delta t) = \Omega_F[t] + \delta\Omega_F \qquad (3)$$

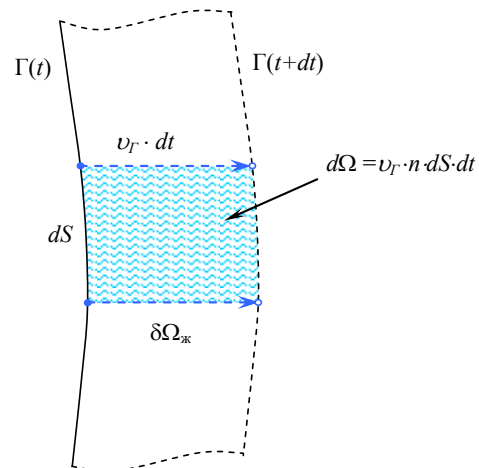**Figure 2.** Changes in subdomain $\Omega_F(t)$, associated with Γ motion.

Figure 3. Interrelation of elementary volume $d\Omega \in \delta\Omega_F$ with Γ local boundary motion parameters.

Here, local volume variation sign associated with the point on Γ would be determined by scalar product $(\upsilon_\Gamma \cdot n)$. Applying relation (3), derivative (2) could be the following:

$$\frac{1}{\Delta t}\left(\int_{\Omega_F[t+\Delta t]}\rho_F[t+\Delta t]d\Omega - \int_{\Omega_F[t]}\rho_F[t]d\Omega\right) =$$
$$= \frac{1}{\Delta t}\left(\int_{\Omega_F[t]}\rho_F[t+\Delta t]d\Omega - \int_{\Omega_F[t]}\rho_F[t]d\Omega\right) + \frac{1}{\Delta t}\left(\int_{\delta\Omega_F}\rho_F[t+\Delta t]d\Omega\right). \qquad (4)$$

The second term in equation (2) is also transformed:

$$\int_{\partial\Omega_F(t)}\rho_F(t)\cdot(\upsilon - \upsilon_\Gamma)\cdot n\cdot dS = \int_{\partial\Omega_F[t]}\rho_F(t)\cdot\upsilon\cdot n\cdot dS - \int_{\partial\Omega_F[t]}\rho_F(t)\cdot\upsilon_\Gamma\cdot n\cdot dS \qquad (5)$$

Based on equation (1), from equations (4) and (5) it can be inferred that:

$$\frac{1}{\Delta t}\left(\int_{\Omega_F[t]}\rho_F[t+\Delta t]d\Omega - \int_{\Omega_F[t]}\rho_F[t]d\Omega\right) + \int_{\partial\Omega_F[t]}\rho_F[t]\cdot\upsilon\cdot n\cdot dS +$$

$$+ \frac{1}{\Delta t}\left(\int_{\delta\Omega_F}\rho_F[t+\Delta t]d\Omega\right) - \int_{\partial\Omega_F[t]}\rho_F[t]\cdot\upsilon_\Gamma\cdot n\cdot dS = 0. \tag{6}$$

Assuming $\Delta t\to 0$, equation (6) is:

$$\frac{\partial}{\partial t}\int_{\Omega_F[t]}\rho_F(t)d\Omega + \int_{\partial\Omega_F[t]}\rho_F(t)\cdot\upsilon\cdot n\cdot dS +$$

$$+ \left\{\lim_{\Delta t\to 0}\left(\frac{1}{\Delta t}\left(\int_{\delta\Omega_F}\rho_F[t+\Delta t]d\Omega\right)\right) - \int_{\partial\Omega_F[t]}\rho_F[t]\cdot\upsilon_\Gamma\cdot n\cdot dS\right\} = 0. \tag{7}$$

The first and second terms in equation (7) represent mass conservation law for fixed subdomain Ω_F at point of time t. This fact explains why the transformation from total derivative $\frac{d}{dt}$ to partial derivative $\frac{\partial}{\partial t}$ has happened. The third term of equation (7) in brackets $\{...\}$ is governed by boundary motion $\partial\Omega_F$. In the volume integral, under sign $\lim_{\Delta t\to 0}$, the elementary volume $d\Omega\in\delta\Omega$ is associated with Γ local motion parameters (figure 3) as:

$$d\Omega=\upsilon_\Gamma\cdot n\cdot dS\cdot dt \tag{8}$$

If $\Delta t\to 0$ average volume density $\rho_F[t+\Delta t]$ (on $d\Omega\in\delta\Omega_F$) would tend to average local density $\rho_F[t]$ within Γ neighborhood. Thus, based on relation (8), it could be concluded:

$$\lim_{\Delta t\to 0}\left(\frac{1}{\Delta t}\int_{\delta\Omega_F}\rho_F[t+\Delta t]d\Omega\right) - \int_{\partial\Omega_F[t]}\rho_F[t]\cdot\upsilon_\Gamma\cdot n\cdot dS = 0. \tag{9}$$

Based on above-mentioned results, equation (9) could be transformed into:

$$\frac{d\Omega_F}{dt} - \int_{\partial\Omega_F[t]}\upsilon_\Gamma\cdot n\cdot dS = 0 \tag{10}$$

Thus, if equation (10) is satisfied, then equation (1) could be written according to Eulerian approach:

$$\frac{\partial}{\partial t}\int_{\Omega_F[t]}\rho_F(t)d\Omega + \int_{\partial\Omega_F[t]}\rho_F(t)\cdot\upsilon\cdot n\cdot dS = 0. \tag{11}$$

Analogue transformation could be applied for impulse and energy conservation laws.

For equation (1), boundary conditions for velocity on the boundary of moving subdomain Ω_F are:

$$\upsilon = \upsilon_\Gamma \text{ on } \partial\Omega_F \tag{12}$$

which mean that fluid does not flow through $\partial\Omega_F$. Under consideration of fixed $\partial\Omega_F$ (it corresponds to equation 11) boundary condition (12) indicates that the fluid moves through $\partial\Omega_F$ at velocity of υ_Γ. In this case, $\partial\Omega_F$ remains fixed only in the time interval $[t; t+\Delta t]$. Afterwards, its position is adjusted to satisfy equation (10). The new position of $\partial\Omega_F$ would correspond to point of time $t+\Delta t$.

Boundary motion velocity of $\partial\Omega_F$ is defined by the solution of solid phase motion problem. In general, corresponding non-stationary, geometrically non-linear equation system should be written in Cartesian coordinates, including:

– solid body motion equation for elementary volume:

$$\rho_S \ddot{u}_i = \left(\sigma_{kj} \left(\delta_{ij} + u_{i,j} \right) \right)_{,k} \tag{13}$$

– deformation tensor components:

$$\varepsilon_{ij} = \frac{1}{2} \left(u_{i,j} + u_{j,i} + u_{l,i} u_{l,j} \right) \tag{14}$$

– interrelations between stress tensor and deformation tensor components:

$$\sigma_{ij} = \sigma_{ij} \left(\varepsilon_{lm} \right) \tag{15}$$

where, ρ_s – density; u – displacement vector of solid body point; σ and ε – stress and deformation tensors, respectively.

According to boundary conditions, boundary $\partial \Omega_S$ could be divided into:

– $\partial \Omega_S^D \in \partial \Omega_S$, under Dirichlet conditions (displacement):

$$u(t,x) = u^{boundary}(t,x), \; x \in \partial \Omega_S^D \tag{16}$$

– $\partial \Omega_S^N \in \partial \Omega_S$, under Neumann conditions (stress):

$$n_k \sigma_{kj} \left(\delta_{ij} + u_{i,j} \right) = p_i^n(t,x), \quad x \in \partial \Omega_S \tag{17}$$

where, $x = \{x_1, x_2, x_3\}$ – vector defined the point on the boundary $\partial \Omega_S$; $u^{boundary}(t, x)$ – function of given displacements; $p_i^n(t,x)$ – load on the boundary point of $\partial \Omega_S$, characterized by normal vector $n = \{n_1, n_2, n_3\}$.

Conjugate problem statement includes continuity conditions on Γ:

– for velocity:

$$\upsilon(x,t) = \dot{u}(x,t), \quad x \in \Gamma(t) \tag{18}$$

– for stress:

$$\tau n = \sigma n, \quad x \in \Gamma(t) \tag{19}$$

where, τ – viscous stress tensor; σ – elastic stress tensor.

3. Conjugate problem solution algorithm for time interval t, $t+\Delta t$

It is presupposed that it is possible to solve independent subtasks in subdomains Ω_F and Ω_S. The solution could be presented by the nodal values of vectors V, P, U, $\dot{U}$ on grids, covering subdomains Ω_F and Ω_S: $\upsilon \rightarrow V$, $P \rightarrow P$, $u \rightarrow U$, $\dot{u} \rightarrow \dot{U}$.

The algorithm is as follows:

1. At point of time t, the vectors V^t, P^t, U^t, $\dot{U}^t$ are known, as well as the Γ^t position.
2. Subtask of fluid flow within $\Omega_F(t)$ is solved i.e. based on V^t, P^t, and Γ^t, vectors $V^{t+\Delta t}$ and $P^{t+\Delta}$ are calculated using relevant vector components of $\dot{U}^t$ on Γ^t
3. From $V^{t+\Delta t}$ and $P^{t+\Delta t,}$ vector of surface nodal forces $F^{t+\Delta t,}$ where fluid acts on the solid body Γ^t surface, is calculated.
4. Elastic subtask within subdomain $\Omega_S(t)$ is solved based on Neumann conditions involving forces $F^{t+\Delta t}$, where the results are $U^{t+\Delta t}$, $\dot{U}^{t+\Delta t}$ and $\Gamma^{t+\Delta t}$.

5. If $\left|X^{t+\Delta t} - X^t\right| < \varepsilon$ is satisfied where X −V and P vectors, then the conjugate problem at point of
    time $t+\Delta t$ is solved. Otherwise, go to step 2, as vectors V, P, U and Γ return to V^t, P^t, U^t and Γ^t;
    however, $\dot U$ remains as $\dot U^{t+\Delta t}$.

6. Subdomain transformation $\Omega_F(t) \rightarrow \Omega_F(t+\Delta t)$ is accomplished by adjusting BI nodes ($\Gamma^t \rightarrow \Gamma^{t+\Delta t}$)
    and further displacement of inner grid nodes and solution interpolation from previous grid (t) to
    new grid ($t+\Delta t$).

Iteration, being performed in step 5, are used to align Γ rate of motion and loads which cause this
motion. It corresponds to conjugate conditions (18) and (19).

In step 6, the method, based on elliptical equation solutions was used to update inner grid node
positions. In this case, it is supposed that the subdomain Ω_F is substituted by solid and elastic
mediums. After this, solid medium stress-strain state is determined if Dirichlet conditions are
displacements of BI nodes located on Γ and defined from elastic problem solution for subdomain Ω_S.

4. Discussion and results
Proposed algorithm was used to solve two tasks. The first task considers adiabatic gas compression in
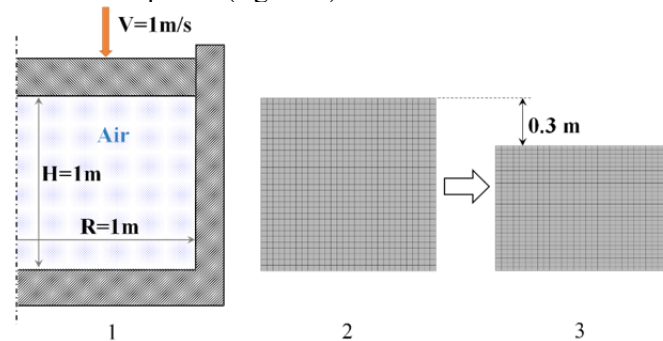a cylindrical vessel with movable piston (figure 4).

Figure 4. Adiabatic gas compression in a cylinder with
non-deformable walls: 1 − geometrical scheme; 2 −
initial grid; 3 − final grid.

The vessel walls and piston are solid (non deformable). The second task investigates the flow
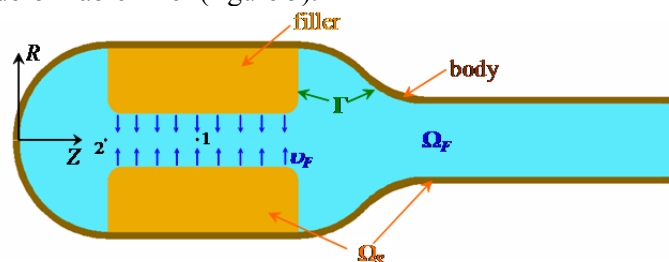injection in a vessel with deformable filler (figure 5).

Figure 5. Axisymmetrical vessel with deformable filler
where the gas flow injection comes out from the filler
channel at velocity υ_F.

Both tasks were axisymmetrically solved. To solve separate subtasks, two independent program
modules were applied. One defined the fluid phase state in the domain with fixed boundaries. The
other was for defining solid phase stress-strain state. The second module was not applied to solve the
first task as the vessel was supposed to be non deformable.

Figure 4 illustrates the first task geometrical scheme, initial grid, covering the calculated domain, and finial grid view under conditions that the vessel piston moved to 0.3 m.

At initial point of time, throughout the calculated domain, the following conditions are:

$$P_{t=0}=1 \cdot 10^5 \text{ Pa}; \ T_{t=0}=273° \text{ K}; \ \upsilon_{t=0}=0 \text{ m/s}.$$

Boundary conditions on the cylindrical vessels walls are:

$$\upsilon_n = 0; \ \frac{\partial P}{\partial n} = 0; \ \frac{\partial T}{\partial n} = 0.$$

where, P, T, υ_n – pressure, temperature and velocity of gas respectively; H - height from the vessel bottom to piston; n – normal vector to vessel walls.

Boundary conditions on piston wall are:

$$\upsilon_n=1 \text{ m/s}; \ \upsilon_n=1 \text{ m/s}; \ P = P_{t=0}\left(\frac{H_{t=0}}{H_t}\right)^{1.4}; \ \frac{\partial T}{\partial n} = 0.$$

The calculation results were compared with well-known analytical relationships for pressure and temperature:

$$P_{analyt} = P_{t=0}\left(\frac{H_{t=0}}{H_t}\right)^{1.4}; \ T_{analyt} = T_{t=0}\left(\frac{H_{t=0}}{H_t}\right)^{0.4}.$$

Moreover, the gas mass M in the vessel should be constant during the compression.

Figure 6 illustrates the dependency of the relative values – mass ($M/M_{t=0}$), pressure (P/P_{analyt}) and temperature (T/T_{analyt}) on time.
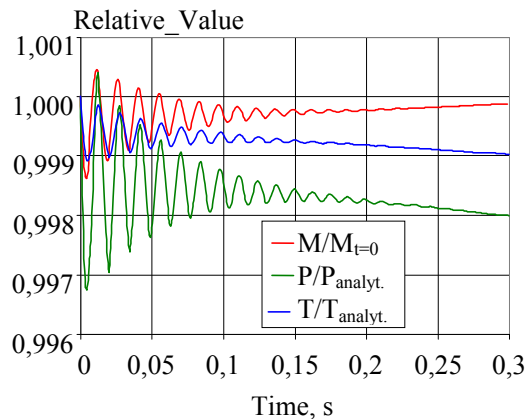

Figure 6. Relative value changes during gas compression in the vessel: mass ($M/M_{t=0}$), pressure (P/P_{analyt}), temperature (T/T_{analyt}).
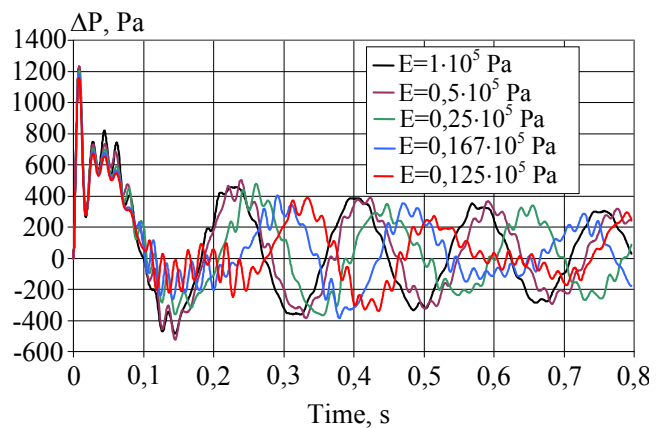
Figure 7. Pressure changes in filler channel at point 1, under different modulus of elasticity values (E) of filler materials ($\Delta P=P-P_{t=0}$).

Numerical values, used to plot the dependency data, correspond to the node positioned close to the vessel wall bottom. These results show a good representation of numerical and analytical solutions relationship because of the fact that ($M/M_{t=0}$), (P/P_{analyt}) and (T/T_{analyt}) are close to unity for considered time interval. It should be noted that proposed conjugate problem solution algorithm maintained the gas mass conservation during its compression in a closed vessel. This can be seen on the dependency graph of $M/M_{t=0}$.

Figure 5 illustrates the geometrical scheme of flow injection in axisymmetrical vessel with deformable filler. In this case, Γ includes not only filler surface, but also vessel wall surface contacting with gas. Domain Ω_S is the volume involving filler and vessel walls.

Tables 1-3 show the geometrical and physical parameters of the second task.

Table 1. Geometrical parameters.

Parameter (m)	Value
Maximum vessel length	10.45
Maximum outer radius	1.5
Vessel wall thickness	0.1
Filler length	3
Channel diameter for filler	0.8
Inner diameter of output channel in the vessel	1.1

Table 2. Material properties.

Property	Vessel walls	Filler
Modulus of elasticity (Pa)	10.45	$(0.125 \div 1.0) \cdot 10^5$
Poisson ratio	0.3	0.3
Density (kg/m^3)	1700	1800

Table 3. Gas properties.

Property	Value
Density (kg/m^3)	1.2
Adiabatic index	1.4
Dynamic viscosity (Pa·s)	$18 \cdot 10^{-6}$
Gas injection velocity (m/s)	0.25

Figure 7 shows how pressure changes within the filler channel at point 1 (figure 5) in time for different filler material modulus of elasticity values.

The presented dependencies show low and high frequencies oscillations. Low frequency can be associated with the filler oscillation as this oscillations period increases, while filler modulus of elasticity decreases. For high frequency oscillations such dependency can not be observed. So, they could be explained by the gas column oscillations in the vessel.

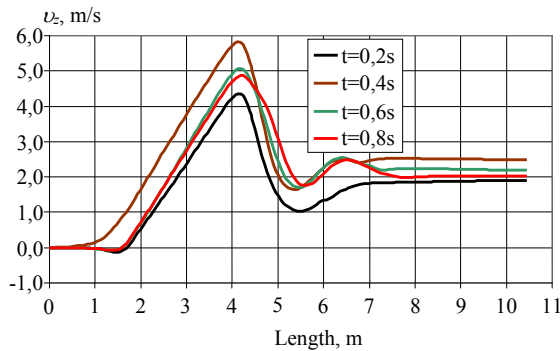Figure 8 shows the distribution of gas velocity along Z axis at different points of time.

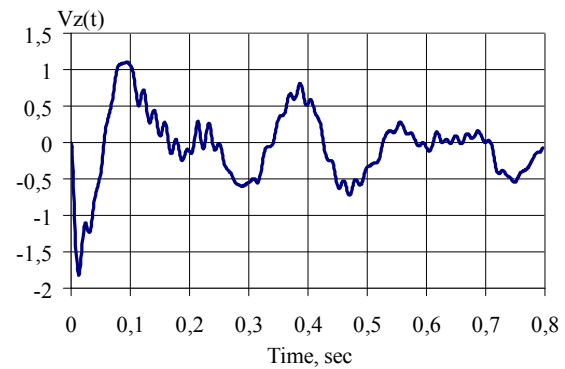**Figure 8.** Distribution of gas velocity along Z axis at different points of time *t*.

Figure 9. Velocity dependency in time at point 2.

The following characteristics of represented dependencies are:
- gas flow velocity near zero at the vessel bottom;
- gas flow acceleration in the filler channel;
- gas flow plugging behind the filler;
- constant flow velocity in vessel channel outlet.

The negative speed region in figure 8 could be explained by the following. It's location at the entrance of the filler channel (indicated as point 2 in figure 5).

The variable flow in this region can be seen in figure 9.

According to figure 9, the velocity Vz(t) sign is changing. This dependency is conditioned by: axial gas oscillations in the channel and filler oscillations.

Figure 10 illustrates the dependencies of gas balance volume Q(t) in time, calculated at point 2.

$$Q(t) = \int_0^t Vz(\tau)d\tau \qquad |Q(t)| = \int_0^t |Vz(\tau)|d\tau$$

The analytical expressions of *Q(t)* are: and .

Value *Q(t)* could be considered as an analog of the gas balance volume flowing in and out of the vessel bottom. Value of *|Q(t)|* is an analog of the whole gas balance volume flowing in or out of the vessel bottom. Figure 10 shows that *Q(t)* value fluctuates near to zero whereas *|Q(t)|* value increases. These dependencies show that gas is flowing in and out of the vessel bottom region constantly. Nevertheless, the mass conservation law is satisfied for this region.

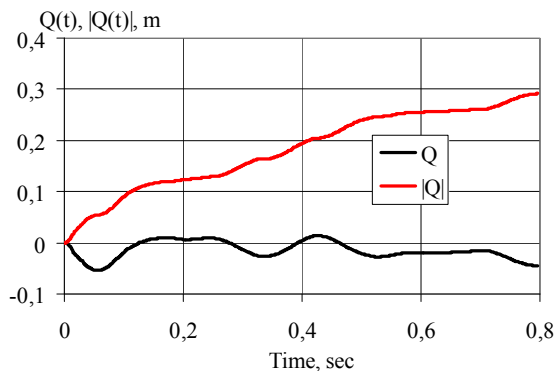Figure 11 shows the dependencies of gas pressure *P(t)* and gas velocity *Vz(t)* in time.

Figure 10. Dependencies of the gas balance volume flowing in and out of the vessel bottom in time at point 2.
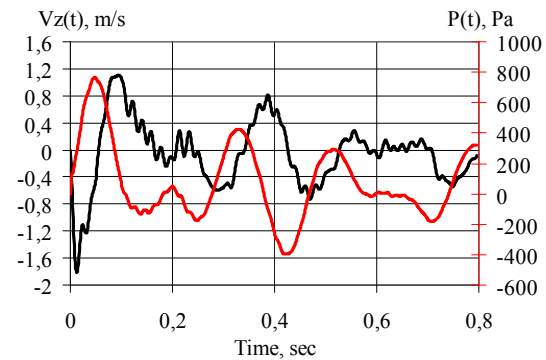

Figure 11. Dependencies of gas pressure *P(t)* and gas velocity *Vz(t)* in time at point 2.

The dependencies in figure 11 indicate physically sound behavior. So, in this case, the data in figure 8 (negative speed values) are reliable.

It should be noted that the difference in distributing axis velocities of gas is governed not only by filler oscillations, but also non-stationary gas flow process in the vessel.

Figure 12 shows deformable filler sections on plane *RZ* at different points of time. Deformation scale on figure 12 is increased. Both radial and axial filler oscillations took place. Moreover, waves extend along the filler surface.

Although there are not comprehensive experimental and analytical data for considered task, the obtained results are not contradictory.
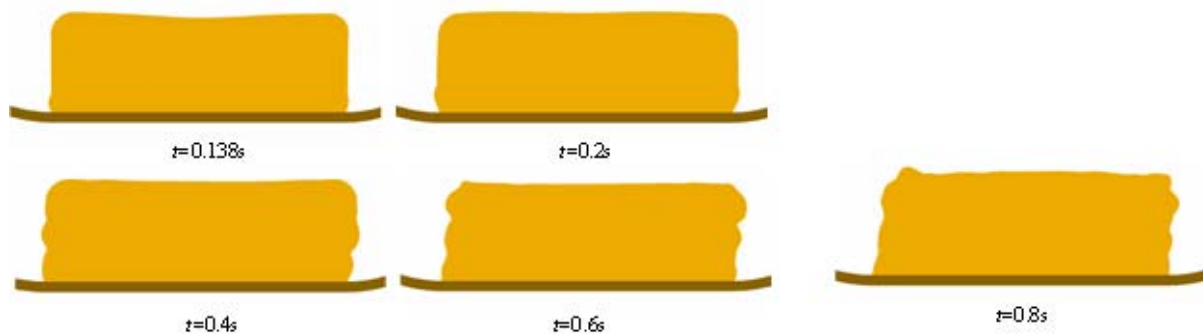

Figure 12. Filler section at different points of time *t* with modulus of elasticity $0.125 \cdot 10^5$ Pa.

5. Conclusion

Proposed conjugate problem solution algorithm for fluid-deformable body system with movable mediums of BI is based on separate subtasks according to the physical principals and conjugate conditions statement between the subtasks.

In determining the fluid phase state, BI is considered to be discrete movable. This means that during the integration step on time, fluid phase BI is not movable, while its motion is substituted by the fluid flow through it. In the next integration step, the boundary has a new position based on calculated solid phase stress-strain state results. When adjusting the BI position and space grid, covering the subdomain of fluid phase, the mass conservation law for fluid phase is satisfied. To solve subtasks, independent program modulus are used. Obtained results are proved the efficiency of proposed algorithm. However, numerical justification are necessary to prove the algorithm efficiency in solving tasks with complex geometry.

References

[1] Kumar M, Kuo K K 1981 Effect of deformation on flame spreading and combustion in propellant cracks *AIAA J.* **19**(12) 1580

[2] Milekhin Yu M, Klychnikov A N, Popov V S, Melnikov V P 2012 Adjoint problem for modeling intraballistic characteristic of solid-propellant rocket motors. *Combust.*, *Expl. Shock Waves.* **48**(1) 33-40

[3] Fiedler R, Jiao X, Namazifard A, Haselbacher A, Najjar F, Parson I D 2001 Coupled fluid-structure 3-D solid rocket motor simulations *AIAA-2001-3954*

[4] Fiedler R A, Breitenfeld M S, Jiao X, Haselbacher A, Geubelle P, Guoy D and Brandyberr M 2002 Simulations of slumping propellant and flexing inhibitors in solid rocket motors,

       AIAA-2002-431

[5]   Engel M, Griebel M 2006 Flow simulation on moving boundary-fitted grids and application to fluid-structure interaction problems *Int. J. Numer. Meth. Fluids* **50** 437

[6]   Puzikova V V, Marchevsky I K 2014 Application of the Ls-Stag immersed boundary method for numerical simulation in coupled aeroelastic problems. *11th World Conf. Comput. Mech, WCCM 2014, 5th Eur. Conf. Comput. Mech., ECCM 2014 and 6th European Conf. on Comput. Fluid Dyn., ECFD 2014* (Barcelona, Spain, Int. Center for Numerical methods in Engineering (CIMNE)) 1995.

[7]   Minakov A V 2014 Numerical algorithm for moving-boundary fluid dynamics problems and its testing *Comput. Math. and Math. Phys.* **54**(10) 1560